

Motion Acoustic Flow Field: Motion Estimation for Blob Targets in Active Sonar Echograph of Harbor Environments

Zhuoqun Wei,¹ Yina Han,^{1, a} Shuang Zhao,¹ Qingyu Liu,² and Jun Song²

¹*School of Marine Science and Technology, Northwestern Polytechnical University, Xi'an 710072, China*

²*Naval Research Academy, Beijing 100161, China*

(Dated: 16 November 2021)

Motion feature is of great significance for blob targets recognition, behavior analysis and threat estimation in active sonar echographs. Hence, it is desirable to access the space-time variation of echo intensity on each spatial-temporal resolution cell from the sonar echographs sequence. Then the subtle motion information of the potential blob targets can be accurately characterized. This idea has been conducted in optical image sequences by solving an motion optical flow field (MOFF) function. Nonetheless, due to the sparkle of the sonar echograph sequences, and strong interferences caused by wake and cavitation noise of fast-moving ship in harbor environments, the constraints underlying the traditional motion optical flow function that is couples the brightness constancy constant along time dimension of each echo intensity points and the motion field spatial smoothness does not hold in our case. Hence, this paper presents a new motion acoustic flow field (MAFF) function and its solving strategy to accurately characterize the subtle motion information of blob targets in active sonar echographs of harbor environments. Experiments on a series of cooperative targets in real-world harbor environments demonstrate the efficacy of our proposed MAFF.

©2021 Acoustical Society of America. [<https://doi.org/DOI number>]

[XYZ]

Pages: 1–10

I. INTRODUCTION

An important goal of sonar system design has been to track and recognize divers or unmanned underwater vehicles (UUVs) to ensure the security of vital military and commercial facilities (Shaw *et al.*, 2005). Given the challenge of hunting these quiet underwater intruders, it is more effective to obtain target echoes from active sonar with high frequency. Generally, sonar returns are normally displayed as an echograph, which reflects the intensity of the echoes in different ranges and bearings (Yang *et al.*, 2012). Owing to the multipath effect, active sonar in harbor environments encounters strong reverberation arising from distributed (rough bottom structures) and discrete (bubbles, fish schools) scatters (Fialkowski *et al.*, 2004; Potter, 2000). High-level scattered returns in an echograph are often easily confused with actual target echoes (Kessel and Hollett, 2006). In addition, as details on the size and appearance signature of quiet underwater intruders are lacking, they exist as blob targets in active sonar echographs. For example, a potential invasion target (a small blob marked by a red rectangle on the active sonar echograph in Fig. 1(a)) may be confused with other light blobs in such sonar echograph, where brighter

blobs indicate higher intensity. Furthermore, diverse invasion targets (the small blob marked by a red rectangle on the active sonar echograph in Fig. 1(a) and Fig. 1(b)) have similar size and appearance signature (light blobs) in sonar echograph, which makes it difficult to effectively distinguish from each other. Thus, there is a need for effective methods to characterize targets in active sonar echographs.

Different from imaging sonar (Lane and Chantler, 1998), the motion feature of blob targets can be effectively characterize targets in active sonar echographs. For example, target tracking is commonly used to refine motion feature into a more useable form at the track level, producing estimates of the likely number of targets and their position, course, and speed. Estimates of target characteristics, such as target type, may also be produced (Mellema, 2018). In addition, if motion feature is available with the other target characteristics and the correlation between a feature value and the target classification is strong, the feature can be used to reject target before tracking (Georgescu and Willett, 2013). SNR and Doppler are commonly used in this role (Georgescu *et al.*, 2011). However, Due to the influence of high level littoral clutters, the direct extraction of blob targets motion information by using the tracker will fail. While the most effective method of motion feature extraction so far is Doppler estimation (Yang *et al.*, 2012; Yu *et al.*, 2017), but in order to overcome the clutter in-

^aElectronic mail: yina.han@nwpu.edu.cn, ORCID: 0000-0001-9713-1821.

interference, these method needs to carry on the fine design of the active sonar transmitting signal. In our previous work, a high-order time lacunarity (HOT-Lac) feature is proposed for detecting potential targets from high level littoral clutters in active sonar echographs (Zhao *et al.*, 2020a), which can obtain motion information of blob targets, but it involves high computational complexity of loop summations. Although the algorithm has been improved in (Zhao *et al.*, 2020b) in later studies, but the new algorithm still has to consume a period of time to accumulate enough frames of sonar echographs for the start of calculation. Hence, motion feature is of great significance for blob targets recognition, behavior analysis and threat estimation in active sonar echographs. It is desirable to access the space-time variation of echo intensity on each spatial-temporal resolution cell from the sonar echographs sequence. Then the subtle motion information of the potential blob targets can be accurately characterized.

This idea has been conducted in optical image sequences by solving an motion optical flow field (MOFF) function in the field of computer vision (Hetherington, 1950; Horn and Schunck, 1981). As a typical optical flow approach, HS method assumed that the brightness of a particular point in the pattern is constant between image sequence and the apparent velocity of the brightness pattern varies smoothly almost everywhere in the image. HS method coupled the brightness constancy and MOFF spatial smoothness assumptions using an energy function called MOFF function, which included data term and spatial term formulated by quadratic both. Based on the HS method, researchers have carried out fruitful researches on solving specific problems of MOFF function, which were fall into two branches. The first branch is to improve the optical flow function in order to enhance its robustness. The early improvement of MOFF function is mainly aimed at the improvement of penalty function. Due to the quadratic penalty function is not robust to outliers, Shulman and Hervé (1989) used an L1 penalty function instead to preserve flow discontinuities. Black and Anandan (1996) used a robust penalty function, Lorentzian, which is a non-convex function. Sun *et al.* (2014) and Bruhn *et al.* (2005) used the Charbonnier, the most robust convex function. The widely used Charbonnier function to penalty a differentiable variant of the absolute value. While the recent work is mainly by improving the local spatial smoothing term. Sun *et al.* (2010, 2014) added a non-local smoothness term to MOFF function, that robustly integrates flow estimates over large spatial neighborhoods. The second branch is to propose efficient and accurate computing frameworks. In terms of efficiency, the current mainstream computing framework is a coarse-to-fine, warping-based approach which is called image pyramid (Bruhn *et al.*, 2005; Sun *et al.*, 2014). Brox *et al.* (2004) theoretically justified the warping-based estimation process. As it is computationally impractical to perform a full search of a image in previous motion optical flow computing frameworks, image pyramid saves computing re-

sources dramatically. In terms of accuracy, one idea is to use *Rudin – Osher – Fatemi* (ROF) structure texture decomposition method Rudin *et al.* (1992) and their linear combinations Sun *et al.* (2010, 2014); Wedel *et al.* (2009). This method effectively resists the influence of brightness changes on the estimation accuracy of motion optical flow. Simpler alternatives, the experimental results show that filter response (or high-order) constancy (Brox *et al.*, 2004; Buades *et al.*, 2005; Sun *et al.*, 2008; Vaudrey and Klette, 2009) can serve the same purpose as ROF texture decomposition. Therefore, the current research does not have a clear conclusion as to which image pre-processing method can achieve better results in different scenarios.

Inspired by the idea of optical flow, we attempted to propose a similar motion field estimation approach to estimate the motion feature of small targets in harbor environments. Nonetheless, due to the sparkle of the sonar echograph sequences, and strong interferences caused by wake and cavitation noise of fast-moving ship in harbor environments, the constraints underlying the traditional motion MOFF function that is couples the brightness constancy constant along time dimension of each echo intensity points and the motion field spatial smoothness does not hold in our case. Thus, the existing optical flow method can not be applied directly in harbor environments. Hence, this paper presents a new motion acoustic flow field (MAFF) function and its solving strategy to accurately characterize the subtle motion information of blob targets in active sonar echographs of harbor environments. The MAFF improves non-local term by adding regularization parameters based on context information, and the pre-processing method is evaluated comprehensively. Furthermore, experiment results on sets of real-world datasets from the South China Sea demonstrate the potential of MAFF in small targets motion feature estimation.

The remainder of the paper is organized as follows. Section II presents the MAFF estimation method. Section III describes the sonar data set used in the experiments. Section IV presents the evaluation metrics, the discussion of the implementation details in MAFF estimation, and performance on small targets motion feature estimation. Our conclusions are presented in Sec. V.

II. MOTION ACOUSTIC FLOW FIELD

A. Motion optical flow field

1. Computation framework of MOFF

Figure 2(a) shows the coarse-to-fine, warping-based computation framework of MOFF. As shown in Fig. 2(a), in each MOFF calculation, image pre-processing is used on two adjacent frames I_t and I_{t+1} in the image sequence, and the pre-processed images $PR(I_t)$ and $PR(I_{t+1})$ are used to construct image pyramid 1 and image pyramid 2 respectively (the green triangle in Figure 2 shows the example of a three-layer image pyramid). Each layer of the image pyramid is recursively down-sampled from its

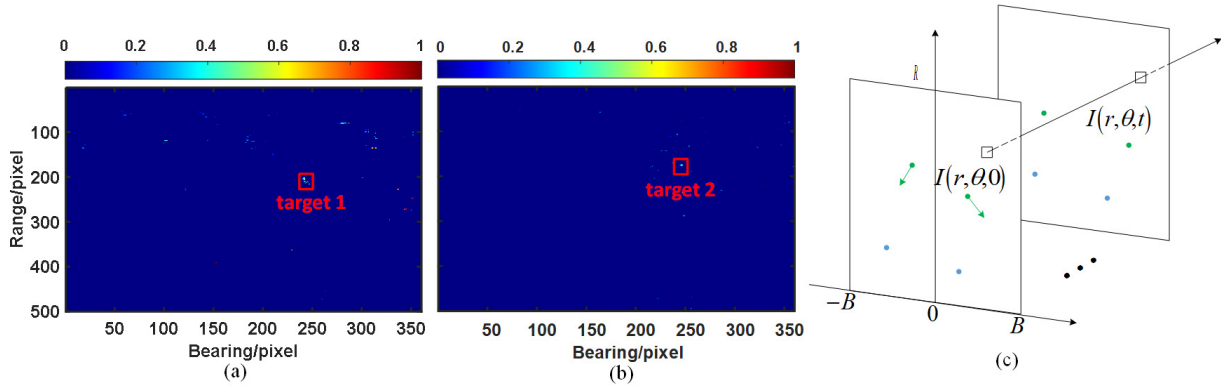


FIG. 1. Active sonar echographs in real-world harbor environments and outline of active sonar echograph sequences: (a) active sonar echograph with potential invasion blob target 1; (b) active sonar echograph with potential invasion blob target 2. Blob target is marked by a red rectangle on the active sonar echograph. (c) outline of active sonar echograph sequence, green spots denote moving blobs and blue spots denote static blobs.

nearest lower layer. The resolution of each layer in the image pyramid decreases with the decrease of the layer's number. MOFF computed at a coarse level is used to warp the second image toward the first at the next finer level. The MOFF is obtained from the top of the pyramid layer by layer, that is, the coarse-to-fine, warping-based computation framework. The operations performed at the bottom of the pyramid are shown on the right of Figure 2(a), which are the same as the calculations in each of the remaining pyramid layers.

2. Motion optical flow function

As shown in Sun *et al.* (2014), the motion MOFF function can be defined as

$$\begin{aligned}
 E(\mathbf{u}, \mathbf{v}) = & \sum_{x=1}^X \sum_{y=1}^Y \rho_D(PR(I_t(x, y))) \\
 & - PR(I_{t+1}(x + u_{x,y}, y + v_{x,y})) \\
 & + \sum_{x=1}^X \sum_{y=1}^Y \lambda_{DS} [\rho_S(u(x, y) - u(x + 1, y)) \\
 & + \rho_S(u(x, y) - u(x, y + 1)) \\
 & + \rho_S(v(x, y) - v(x + 1, y)) \\
 & + \rho_S(v(x, y) - v(x, y + 1))] \\
 & + \lambda_N \sum_{x,y} \sum_{(x', y') \in \mathcal{N}_{x,y}} (|u(x, y) - u(x', y')| \\
 & + |v(x, y) - v(x', y')|), \tag{1}
 \end{aligned}$$

where I_t is a $X \times Y$ image, \mathbf{u} and \mathbf{v} are the horizontal and vertical components of the MOFF, $\mathbf{u} = \{u(x, y) | 1 \leq x \leq X, 1 \leq y \leq Y\}$, $\mathbf{v} = \{v(x, y) | 1 \leq x \leq X, 1 \leq y \leq Y\}$. The first term in Eq. 1 is data term, which assumes brightness constancy, $PR(I_t)$ and $PR(I_{t+1})$ are two image frames, (x, y) indexes a particular image pixel location. The second term in Eq. 1 is spatial term, which

assumes motion optical flow field spatial smoothness, $u_{x,y}$ and $v_{x,y}$ are elements of \mathbf{u} and \mathbf{v} respectively. ρ_D is data penalty function, ρ_S is spatial penalty function

$$\begin{aligned}
 \rho_D(I_s) &= (I_s^2 + \epsilon^2)^a, \\
 \rho_S(I_s) &= (I_s^2 + \epsilon^2)^a, \tag{2}
 \end{aligned}$$

where, $\epsilon = 10^{-3}$, and $a = 0.45$, which are the optimal parameter investigated in (Sun *et al.*, 2014). λ_{DS} is a regularization parameter that balance brightness constancy and motion field spatial smoothness. The last term in Eq. 1 is a non-local term, which imposes a particular smoothness assumption within a specified large region of the motion optical flow field, $\mathcal{N}_{x,y}$ is the set of neighbors of pixel (x, y) in a possibly large area and λ_N is a scalar weight. The non-local term minimizes the L1 distance between the central value and all motion optical flow values in its neighborhood except itself.

B. Motion acoustic flow field

1. Computation framework of MAFF

Figure 2(b) shows the computation framework of MAFF proposed in this paper. Different from the typical MOFF computational framework given in Figure 2 (a), the proposed novel MAFF computation framework optimizes pre-processing module and the spatial smoothing module to hold our case (the red dotted box in Figure 2 (b) shows our method). Firstly, in the echograph pre-processing module, MAFF computation framework adopted the combination pre-processing method, which linearly combined the results of the original echograph and several different pre-processing methods to obtain the final pre-processing results. Specifically, several different pre-processing methods is ranging from ROF structure texture decomposition, Gaussian pre-filter, Laplacian pre-filter, LoG pre-Filter and Sobel edge detector, these methods have been proved to be effective in the

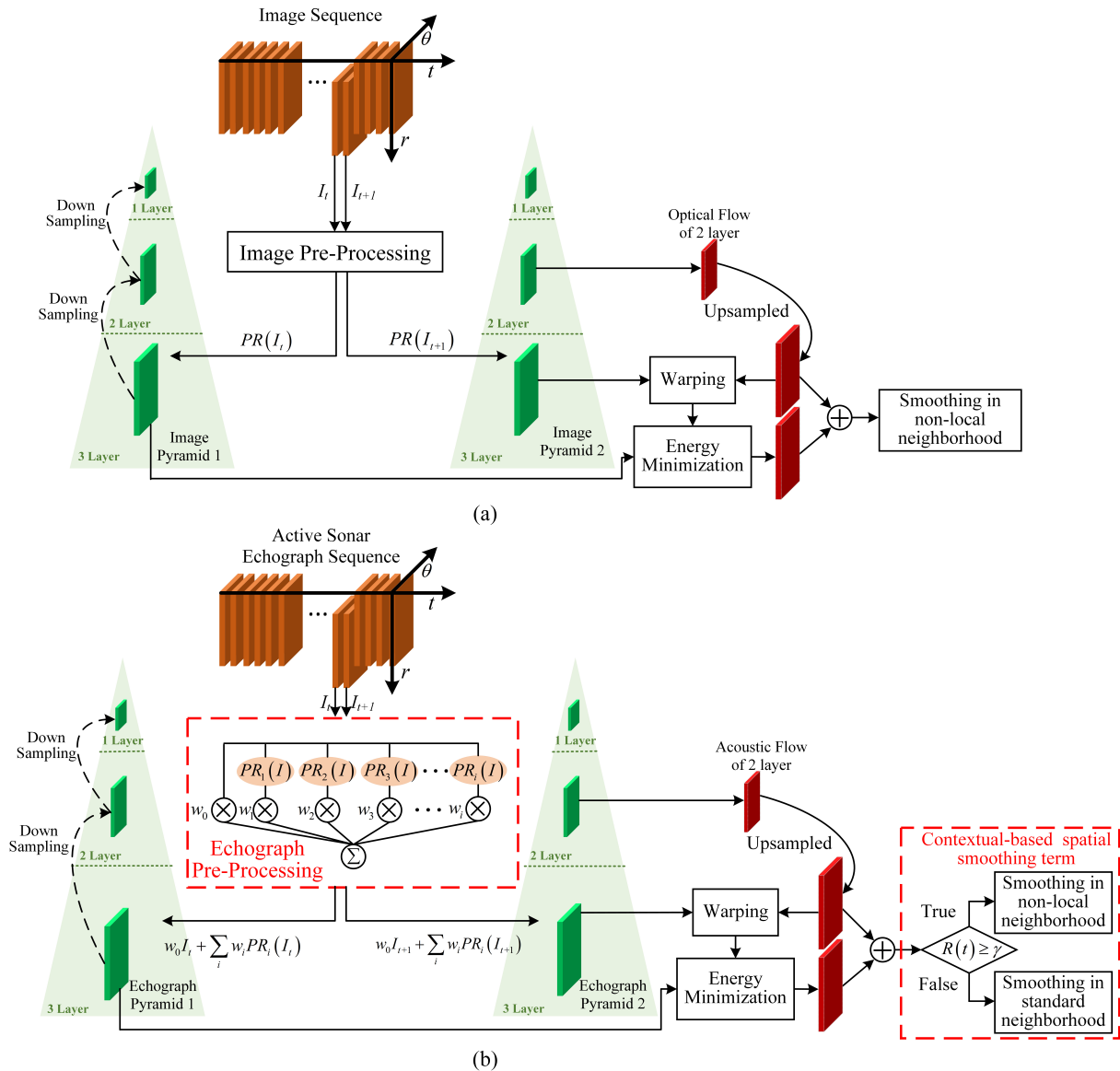


FIG. 2. Computation framework of MOFF and MAFF: (a) Computation framework of MOFF includes fixed image pre-processing and image pyramid processing which MOFF estimated in each pyramid layer is smoothed in non-local neighborhood; (b) Computation framework of MAFF includes combination pre-processing method for echographs and echograph pyramid processing which MAFF estimated in each pyramid layer is smoothed with contextual-based spatial smoothing term.

previous work and our previous experiments. In addition, the weight w_I of the linear combination is determined by experiment, which will be expanded in detail in IV B 2. Secondly, in the spatial smoothing module, we introduce global context information to determine whether to perform global spatial smoothing for MAFF in the non-local neighborhood or in the standard neighborhood. Figure 3 shows the difference between the two neighborhoods, the standard pairwise neighborhood model connects a center pixel with its nearest neighbors, while the non-local term connects a pixel with many pixels in a large spatial neighborhood. The basis for the judgment is formulated in the next section.

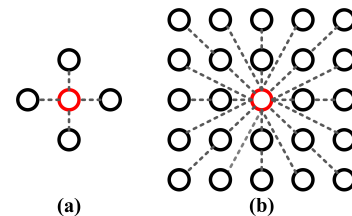


FIG. 3. Neighborhood structure for the center (red) pixel: (a) the standard pairwise neighborhood model; (b) the non-local neighborhood model

2. Motion acoustic flow function

The intensity of the target echo is generally a function of the size of the entity and the severity of the impedance changes, in most cases providing an easily quantifiable measure of its range and bearing from a receiver. The correlativity between incident acoustic intensity and target echo intensity of active sonar is

$$\frac{I_s}{I_i} \propto L^2 \left(\frac{\sin \beta}{\beta} \right)^2 \cos^2 \alpha \quad (3)$$

where I_s is the target echo intensity, I_i is the incident acoustic intensity. L is the length of the longer side of the scatterer, $\beta \propto L \sin \alpha$, where α is the angle between the incident direction of the acoustic wave and the normal direction. As shown in Fig. 1(c), HF active sonar echo signals are displayed as echograph

$$I_t(r, \theta) = I_s(r, \theta, t), \quad (4)$$

where I_t is active sonar echograph at time t , (r, θ, t) represents a certain spatial-temporal resolution cell of sonar. And at the time t , (r, θ) is a certain pixel in sonar echograph. As shown in Figure 2(b), pre-processed sonar echograph is

$$P_t(r, \theta) = w_0 I_t + \sum_i w_i P R_i(I_t(r, \theta)), \quad (5)$$

where w_0 is weight of original echograph, $w_i (i = 1, 2, 3 \dots)$ are weights of pre-processing methods, $P R_i (i = 1, 2, 3 \dots)$ are results of pre-processing methods. The motion acoustic flow function defined as

$$\begin{aligned} E(\mathbf{u}, \mathbf{v}) = & \sum_{r=0}^R \sum_{\theta=-B}^B \rho_D (P_t(r, \theta) - P_{t+1}(r, \theta)) \\ & + \sum_{r=0}^R \sum_{\theta=-B}^B \lambda_{DS} [\rho_S (u(r, \theta) - u(r+1, \theta)) \\ & + \rho_S (u(r, \theta) - u(r, \theta+1)) \\ & + \rho_S (v(r, \theta) - v(r+1, \theta)) \\ & + \rho_S (v(r, \theta) - v(r, \theta+1))] \\ & + \lambda_{N'} \sum_{r, \theta} \sum_{(r', \theta') \in \mathcal{N}_{r, \theta}} \left(\left| u(r, \theta) - u(r', \theta') \right| \right. \\ & \left. + \left| v(r, \theta) - v(r', \theta') \right| \right), \end{aligned} \quad (6)$$

where R and B are the beam and range limits. $\mathcal{N}_{r, \theta}$ is neighborhood of (r, θ) in the sonar echograph, (r', θ') are pixels in $\mathcal{N}_{r, \theta}$. In Eq. 6, an adaptive regularized parameter $\lambda_{N'}$ is used to replace the original fixed regularized parameter $[\lambda_N$ in Eq. 1]. At the time t ,

$$\lambda_{N'} = \begin{cases} 1, & \text{if } R(t) \geq \gamma \\ 0, & \text{if } R(t) < \gamma, \end{cases} \quad (7)$$

where, the threshold γ is the threshold value. As the cavitation noise appear as vertical strips in sonar echograph,

the appearance of fast-moving ships intrude into the detection area will result in a large number of false target points. And γ can be determined by statistical analysis of false target points in the same scenario in the previous experimental data. $R(t)$ is the ratio of foreground pixels of all pixels

$$R(t) = \frac{1}{2B \times R} \sum_{r=-B}^B \sum_{\theta=0}^R I_b(r, \theta, t). \quad (8)$$

To obtain global context information, the sonar echograph is characterized by a binary image whose pixel values are given by

$$I_b(r, \theta, t) = \begin{cases} 1, & \text{if } (r, \theta, t) \in P_F \\ 0, & \text{if } (r, \theta, t) \in P_B, \end{cases} \quad (9)$$

where P_F and P_B are collections of foreground pixels (potential moving pixels) and background pixels (static pixels) respectively which are split by a normal Gaussian mixture model. In this paper, the second and third terms in Eq. 6 are collectively referred to as a spatial smooth term in the motion acoustic flow function.

III. SONAR DATA SET

In our experiment, we use the multi-beam active sonar system with a fixed shore-based platform for harbor monitoring. The periodic acoustic pulse is transmitted into the underwater environment and moving targets and then collected by receiving arrays. An active sonar echograph is a 2D grayscale image composed of received acoustic signals, which are beamformed, match filtered, and normalized. Here, using normalized sonar data after gating tests, we discuss the ability of MAFF to characterize the subtle motion information of blob targets in active sonar echographs of harbor environments. Generally, the performance evaluation data can be obtained through numerical modeling and real experiments. However, both analytical and numerical modeling are difficult because reverberation in real oceans is highly non-Gaussian (Yu *et al.*, 2017). Therefore, real experimental data is used for performance evaluation in this paper. The echographs used in this paper were drawn from real measured sonar data collected from a single region by multiple experiments in the South China Sea in 2015. Specifically, four representative sets of images were collected, containing different moving targets that are of concern in a harbor environment. The targets were chosen to have different echo energy, object size, and motion mode in order to verify the robustness of the proposed feature. These active sonar echographs are shown in Fig. 4 (multi-frame accumulation of active sonar echographs can be obtained by accumulating the echo on each spatial-temporal resolution cell, the echographs are then normalized by echo intensity).

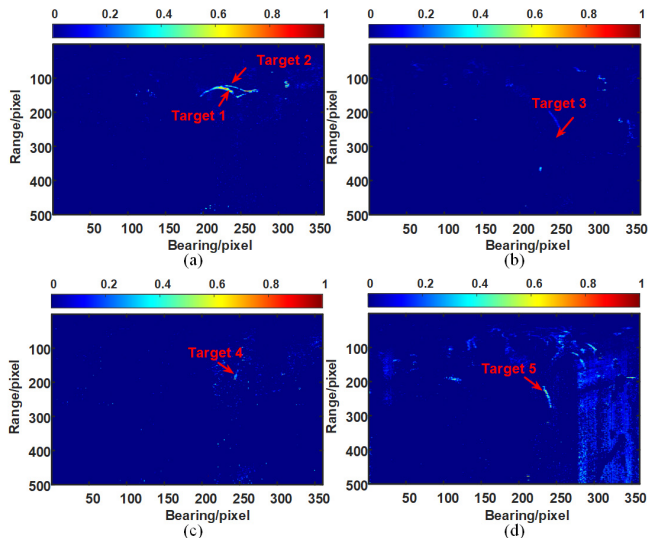


FIG. 4. Normalized multiframe accumulation from active sonar echographs, in which the targets of interest are moving in the red arrows: (a) Data set 1, including 130 frames, Small target 1 towed Small target 2 in a curved motion across the active sonar beam, the echo energy of the Small target 1 was higher than that of the Small target 2; (b) Data set 2, including 80 frames, Small target 3 were moving in an approximately straight line away from the sonar; (c) Data set 3, including 40 frames, Small target 4 was moving in an approximately straight line away from the sonar, with this motion being slower than that of the targets in Data set 2; (d) Data set 4, including 188 frames, Small target 5 also moved in an approximately straight line away from the sonar.

IV. EXPERIMENTAL EVALUATION

A. Evaluation metrics

The aim of this paper was to evaluate whether the MAFF could accurately characterize the subtle motion information of blob targets in active sonar echographs of harbor environments. In consideration of the practical needs of motion information observation, we explicitly show the motion information by coding the MAFF with a specific color key. For example, Fig. 5 (a) shows vector (u, v) in MAFF, consider the polar coordinates case:

$$\begin{aligned} |(u, v)| &= \sqrt{u^2 + v^2} \\ \phi &= \arctan \frac{v}{u}, \quad 0 \leq \phi \leq 2\pi, \end{aligned} \quad (10)$$

where $|(u, v)|$ is the speed of blob target moving on active sonar echograph, ϕ is direction of motion. As shown in Fig. 5(b), the magnitude and direction of flow can be uniquely mapped to color saturation and hue in the color key map. Nevertheless, subtle visual differences usually affect the judgment of the motion information of the blob targets. Hence, the industry usually uses the motion flow field estimation error for quantitative assessment. Generally, flow field estimation error can be measured in

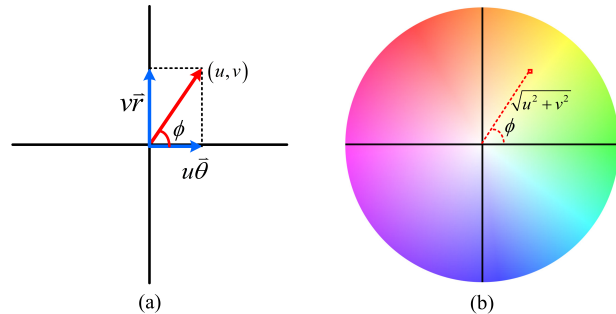


FIG. 5. (a) MAFF in cartesian coordinates; (b) MAFF in polar coordinates, define a color key of MAFF, (\mathbf{u}, \mathbf{v}) has a unique mapping in the color key map, that is, to distinguish the different direction of motion by hue, to distinguish the speed of motion by color saturation.

two main ways. One is to obtain average angular error (AAE) and average end-point error (EPE) by comparing estimated motion flow field with ground truth motion flow field. Another is the forward-backward error (FBE) (Plyer *et al.*, 2015; Xiang *et al.*, 2019), which is a way to compute flow field estimation error without ground truth motion flow field. In our experiment, it is almost impossible to obtain the ground truth motion flow field, because it is difficult to manually label the correct pixel wise correspondences of active sonar echographs measured in real experiments data even if the prior information such as speed and direction of targets have been known. Therefore, we use average forward-backward error (AFBE) for quantitative assessment. AFBE of frame t in echograph sequence is

$$\begin{aligned} \text{FBE}_t &= \frac{1}{2B \times R} \sum_{r=-B}^B \sum_{\theta=0}^R \left| \vec{u}(r, \theta) + \overleftarrow{u}(r, \theta) \right. \\ &\quad \left. + \vec{v}(r, \theta) + \overleftarrow{v}(r, \theta) \right|, \end{aligned} \quad (11)$$

where, $(\vec{u}(r, \theta), \vec{v}(r, \theta))$ is estimated by the pixel (r, θ) in the frame t to its corresponding pixel in the frame $t + 1$, and $(\overleftarrow{u}(r, \theta), \overleftarrow{v}(r, \theta))$ is estimated by the pixel (r, θ) in the frame $t + 1$ to its corresponding pixel in the frame t . As shown in Figs. 6(a) and (b), the forward MAFF $(\vec{\mathbf{u}}, \vec{\mathbf{v}})$ ($\vec{\mathbf{u}} = \{\vec{u}(r, \theta) | 0 \leq r \leq R, -B \leq \theta \leq B\}$, $\vec{\mathbf{v}} = \{\vec{v}(r, \theta) | 0 \leq r \leq R, -B \leq \theta \leq B\}$) and the backward MAFF $(\overleftarrow{\mathbf{u}}, \overleftarrow{\mathbf{v}})$ ($\overleftarrow{\mathbf{u}} = \{\overleftarrow{u}(r, \theta) | 0 \leq r \leq R, -B \leq \theta \leq B\}$, $\overleftarrow{\mathbf{v}} = \{\overleftarrow{v}(r, \theta) | 0 \leq r \leq R, -B \leq \theta \leq B\}$) are reversed. The forward-backward error is the sum of forward MAFF and backward MAFF, which is zero theoretically [Fig. 6(c)]. It's worth noting that we use normalized multiframe accumulation of coded MAFF to construct MAFF map to display the motion information of the blob target in the multi-frame sonar echograph in a single graph.

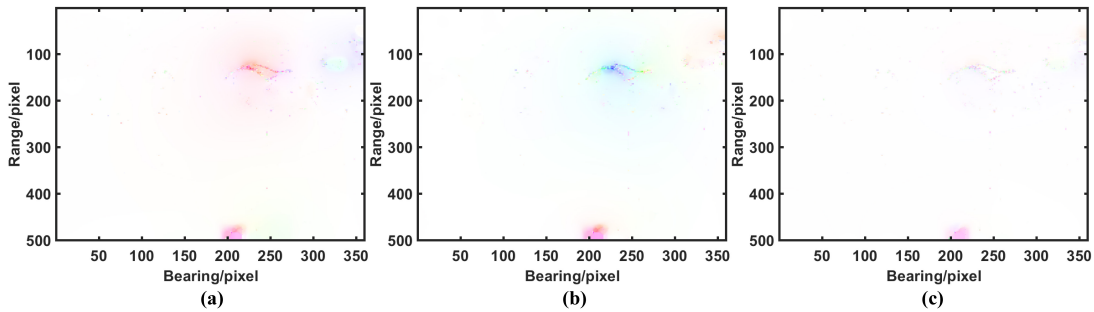


FIG. 6. MAFF map (normalized multiframe accumulation of coded MAFF): (a) the forward MAFF map, the displacements from the pixels in frame t to their corresponding pixels in the frame $t + 1$; (b) the backward MAFF map, the displacements from the pixels in frame $t + 1$ to their corresponding pixels in the frame t ; (c) the forward-backward error (FBE), the sum of forward MAFF and backward MAFF, that an ideal correspondence should be zero.

B. Ablation experiments: discussion of the implementation details in MAFF estimation

The main innovations of this paper are combination pre-processing method and contextual based MAFF spatial smoothing method. In order to analyze the enhanced motion estimation accuracy achieved by our work, in this section we introduce the concept of ablation analysis, a procedure investigation that is conducted by starting from a basic configuration then iteratively modifying one setting of the model and seeing how that affects performances on the sonar datasets. Specifically, in Sec. IV B 1, we discuss the ability of combination pre-processing method with spatial smoothing method based on non-local term, while in Sec. IV B 2, we discuss the ability of contextual based MAFF spatial smoothing method with combination pre-processing method. The real experimental data and evaluation metrics introduced in Sec. III and Sec. IV A will be used in this section.

1. Pre-processing method

In this part, the pre-processing method in estimation framework of MAFF from the perspective of the accuracy of MAFF estimation are discussed. To gain accurate estimation of optical flow field against brightness changes ROF structure texture decomposition method to reduce the influence of illumination changes between frames. As the improvement linearly combined the texture and structure components (in the proportion 20:1). Simpler alternatives, a variety of pre-filters had been used in previous research, for example, Laplacians pre-filter boosted the high frequency while suppressing the low frequency components that contain the lighting change. Nevertheless, Laplacians pre-filter is sensitive to noise. Gaussians pre-filter has good performance in denoising, but it could easily over-smooth image sequences. Meanwhile, Gaussians pre-filter performed well on processing the synthetic image sequences, but poorly on real ones. The LoG filter combined the advantages of these two, and could be generated by taking the Laplacian of the Gaussian kernel. Furthermore, edges had also been emphasized using the

Sobel edge magnitude, but appeared to not work well on some image sequences, particularly the synthetic ones (Sun *et al.*, 2014).

Specifically, MAFF estimation approach without pre-processing is the basic configuration in this part, which is defined as a baseline model 1. Based on Baseline Model 1, the pre-processing method is iteratively modified, including ROF structure texture decomposing, Gaussian pre-filtering, Laplacian pre-filtering, LoG pre-filtering and Sobel edge detecting. For each modification, the estimation accuracy that evaluated by AFBF for each group of targets is shown in Table I. The Bold entries highlight the optimal pre-processing method. Comparing the average AFBF for each modification, it can be seen that the LoG pre-filtering method provides the best performance of MAFF estimation. This can be attributed that LoG is robust to Gaussian noise while highlighting the edges of the target.

However, for each group of targets, owing to the different motion modes, there exists an optimal pre-processing method. Specifically, the ROF structure texture decomposition provides the lowest value of AFBF for Data set 1, which has more curves in the trajectory. The minimum value of AFBF for Data sets 2 to 4 exists on the pre-processing method of LoG pre-filter. As shown in Table I, the sobel edge detector achieves highest AFBFs whether in each individual data set or the average, which are significantly worse than the baseline approach. And Gaussian pre-filter and Laplacian pre-filter gains the similar performance, that neither of these methods differ significantly from the approach without pre-process. These results suggest that although constant target edge is very important for subsequent processing, but the pre-processing method that simply detects the edge without considering the influence of noise will often get worse results than that without pre-processing.

2. Spatial smoothing term

In this part, we will provide some insight into how the MAFF estimation accuracy varies as the spatial smoothing term changes. Owing to the fast-moving ships that

TABLE I. AFBFs of different pre-processing methods.

	Data set				
	Data 1	Data 2	Data 3	Data 4	Average
No pre-process	0.0169	0.0154	0.0227	0.1288	0.04595
ROF structure texture decomposition	0.0052	0.0061	0.0071	0.0155	0.0085
Gaussian pre-filter	0.0128	0.0139	0.0134	0.0413	0.02035
Laplacian pre-filter	0.0134	0.0150	0.0138	0.0191	0.01533
LoG pre-filter	0.0062	0.0053	0.0070	0.0150	0.00838
Sobel edge detector	0.0376	0.0332	0.0594	0.1390	0.0673

are not of interest intrude into the detection area, additional motion acoustic flow caused by the ship and its following stern wake was introduced artificially into the motion estimation of a interested target. As the wake and cavitation noise of fast-moving ship coexist with the target of interest in sonar echograph, the assumption of velocity of the brightness pattern varies smoothly within a large neighborhood will cause loss of target motion feature. The motion optical flow of small target has no absolute dominant position in the high level littoral background, which is easy to assimilate.

As shown in Table I, the AFBFs of Data set 4 are significantly higher than others. To provide further detail, we explicitly show the MAFF of small target 5 that include the frame with additional fast-moving ship and without additional fast-moving ship, as shown in Fig 7. The target in Fig 7(a) is "clearer" than that in Fig 7(b). It is because of the role of non-local term in the motion acoustic flow function, which resulting in a large spatial smoothing neighborhood. Nonetheless, the motion acoustic flow of small target can assimilate due to it has no absolute dominant position compared with additional fast-moving ship, as shown in Figs 7(c)-(d).

In order to analyze the improvement in MAFF estimation accuracy achieved by context-based non-local spatial smoothing term, AFBFs of MAFF estimation approach with different spatial smoothing term in motion acoustic flow function are further calculated. Motion acoustic flow function with non-local term is the basic configuration in this part (as 1), which is defined as a baseline model 2. For each group of targets, we optimize the pre-processing method by the results of Sec. IV B 1. Based on Baseline Model 2, the spatial smoothing term in motion acoustic flow function is iteratively modified, including simply removing non-local term and contextual-based non-local term. As shown in Table II, approach with contextual-based non-local term in motion acoustic flow function achieves the lowest AFBFs among each approach. Comparing the AFBFs for each approach, it can be seen that as the motion estimation performance of Data set 4 achieves the biggest improvement, although it is also poorer than that of other Data sets.

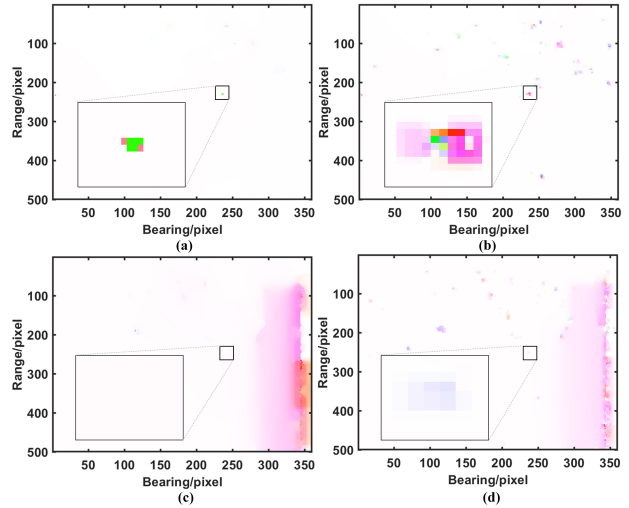


FIG. 7. MAFF of small target 5: (a) w/o non-local term & w/o fast-moving ship; (b) With non-local term & w/o fast-moving ship; (c) w/o non-local term & with fast-moving ship; (d) With non-local term & with fast-moving ship. Magnified versions of the black box given in the lower left corner of the image.

C. Experiments results assessment: performance on small targets motion estimation

The results so far have indicated that proposed MAFF estimation approach has an improved accuracy than the motion optical flow approach. The following is the discussion on the application potential of the propose approach. The aim of this paper was to evaluate whether the modified motion acoustic flow function and calculate framework could effectively improve the estimated accuracy of the existing motion optical flow approach. In consideration of the practical needs of motion estimation, we explicitly show the MAFF maps (Normalized multi-frame cumulative MAFF) from the four data sets in Fig. 7.

As shown in Fig. 7(e), the target 1 and 2 can be highlighted on a MAFF map in the form of a track, and more motion details are resumed compared with MAFF map

TABLE II. AFBFs of the different spatial smoothing term.

Spatial smoothing term	Data set				Average
	Data 1	Data 2	Data 3	Data 4	
With non-local term	0.0052	0.0053	0.0070	0.0150	0.00813
w/o non-local term	0.0118	0.0142	0.0101	0.0232	0.01483
Contextual-based non-local term	0.0050	0.0048	0.0065	0.0084	0.00618

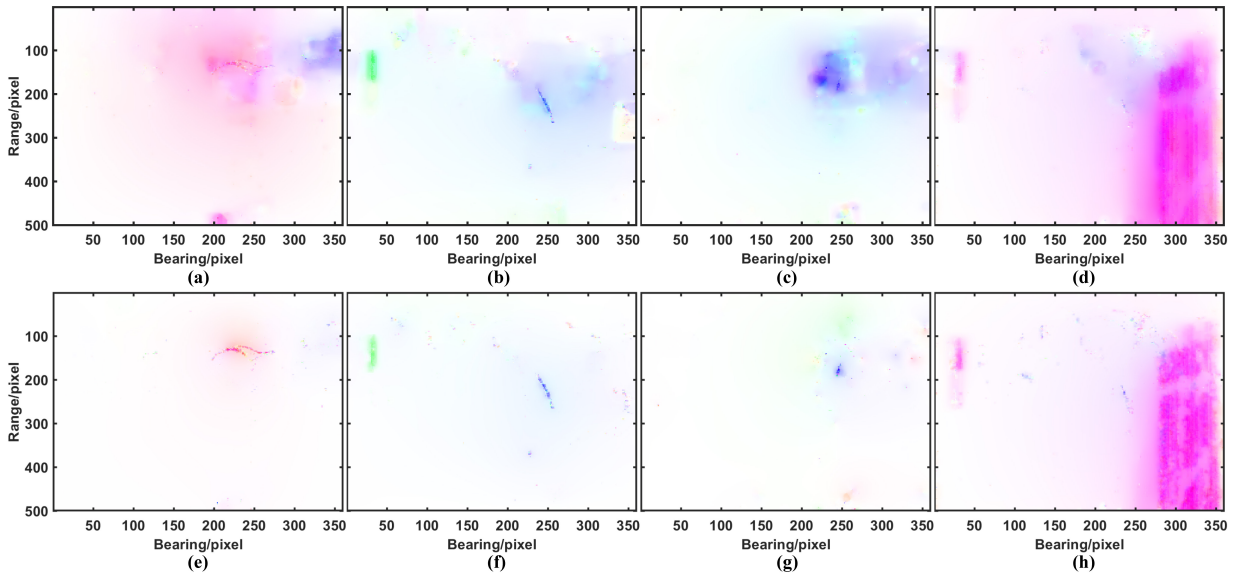


FIG. 8. MAFF maps coded by different flow estimation approaches, (a) to (d) are the proposed MAFF estimation approach, (e) to (h) are the motion optical flow approach

estimated with motion optical flow approach in Fig. 7(a). Moreover, the number of pixels covered by moving clutter background is significantly reduced. Similarly, the proposed approach achieved higher accuracy in target 3 and 4, which move in straight lines in sonar echograph, as shown in Fig. 7(b)(c)(f) and (g). As shown in Fig. 7(d) and (h), the performance difference between the proposed approach and motion optical flow approach shows up after the intrude of fast-moving ship. The proposed approach preserves more motion feature of the target to avoid its MAFF being masked.

The fine motion details are shown in MAFF maps real-time updated. The estimated initial range and speed information of the interested target in the detection area can be used as stated parameters for the extended Kalman filter (EKF) (Duan *et al.*, 2014). On the other hand, object segmentation at object level need the motion feature as prior (Brox and Malik, 2010). With growing interest in using unsupervised learning for underwater target recognition, a high accuracy and robustness motion flow estimator may be used as input for subsequent processing.

V. CONCLUSION

In this paper, a novel feature, MAFF, for characterizing the targets' motion mode in active sonar echograph of harbor environment are presented. The MAFF maps detect and preserve fine motion details of weak targets in real-world harbor environments in the South China Sea. In our experiment, the robustness of proposed method is tested by a series of targets in four data sets. In addition, the accuracy of MAFF estimation has been improved by new motion acoustic flow function with contextual-based non-local term and the calculation framework with pre-processing methods for sonar echograph.

ACKNOWLEDGMENTS

This work was supported in part by the National Key RandD Program of China under Grant No. 2016YFC1400200, in part by the National Natural Science Foundation of China under Grant No. 61671388, and in part by the National Engineering Laboratory for Integrated Aero Space-Ground-Ocean Big Data Application Technology.

- Black, M. J., and Anandan, P. (1996). “The robust estimation of multiple motions: Parametric and piecewise-smooth flow fields,” *Computer Vision & Image Understanding* **63**(1), 75–104.
- Brox, T., Bruhn, A., Papenberger, N., and Weickert, J. (2004). “High accuracy optical flow estimation based on a theory for warping,” in *Proceedings of the European Conference on Computer Vision (ECCV)*, pp. 25–36.
- Brox, T., and Malik, J. (2010). “Object segmentation by long term analysis of point trajectories,” in *Proceedings of Computer Vision—ECCV 2010: 11th European Conference on Computer Vision, Heraklion, Crete, Greece, September 5–11, 2010, Part V*.
- Bruhn, A., Weickert, J., and Schnörr, C. (2005). “Lucas/Kanade Meets Horn/Schunck: Combining local and global optic flow methods,” *International Journal of Computer Vision* **61**(3), 211–231.
- Buades, A., Coll, B., and Morel, J.-M. (2005). “A non-local algorithm for image denoising,” in *2005 IEEE Computer Society Conference on Computer Vision and Pattern Recognition (CVPR’05)*, IEEE Computer Society Press, Vol. 2, pp. 60–65.
- Duan, R., Yang, K., Ma, Y., Yang, Q., and Li, H. (2014). “Moving source localization with a single hydrophone using multipath time delays in the deep ocean,” *Journal of the Acoustical Society of America* **136**(2), EL159–EL165.
- Fialkowski, J. M., Gauss, R. C., and Drumheller, D. M. (2004). “Measurements and modeling of low-frequency near-surface scattering statistics,” *IEEE Journal of Oceanic Engineering* **29**(2), 197–214.
- Georgescu, R., and Willett, P. (2013). “The gmcpd tracker applied to the clutter09 dataset,” in *Information Fusion (FUSION), 2013 16th International Conference on*.
- Georgescu, R., Willett, P., and Schoenecker, S. (2011). “Gm-cphd and ml-pda applied to the metron multi-static sonar dataset,” in *2010 13th International Conference on Information Fusion*.
- Hetherington, R. (1950). *The perception of the visual world* (Houghton Mifflin,).
- Horn, B. K. P., and Schunck, B. G. (1981). “Determining optical flow,” *Artificial Intelligence* **17**(1-3), 185–203.
- Kessel, R. T., and Hollett, R. D. (2006). “Underwater intruder detection sonar for harbour protection: state of the art review and implications,” *Underwater Intruder Detection Sonar for Harbour Protection State of the Art Review & Implications*.
- Lane, D. M., and Chantler, M. J. (1998). “Robust tracking of multiple objects in sector-scan sonar image sequences using optical flow motion estimation,” *IEEE Journal of Oceanic Engineering* **23**(1), 31–46.
- Mellema, G. R. (2018). “Improved active sonar tracking in clutter using integrated feature data,” *IEEE Journal of Oceanic Engineering* **PP**(99), 1–15.
- Plyer, A., Colin-Koeniguer, E., and Weissgerber, F. (2015). “A new coregistration algorithm for recent applications on urban SAR images,” *IEEE Geoscience & Remote Sensing Letters* **12**(11), 2198–2202.
- Potter, J. R. (2000). “Challenges of seeing underwater - a vision for tomorrow,”.
- Rudin, L. I., Osher, S., and Fatemi, E. (1992). “Nonlinear total variation based noise removal algorithms,” *Physica D Nonlinear Phenomena* **60**(1-4), 259–268.
- Shaw, K., Scott, R., and Holdanowicz, G. (2005). “Sonar sentinels on guard for submerged swimmers,” *Janes Navy International* **110**(8), p.10–12,14,16–18.
- Shulman, D., and Hervé, J.-Y. (1989). “Regularization of discontinuous flow fields,” in *Proceedings of Workshop on Visual Motion, Irvine, CA, USA, March 20–22*, IEEE Computer Society Press, pp. 81–86.
- Sun, D., Roth, S., and Black, M. (2010). “Secrets of optical flow estimation and their principles,” **1**, 2432–2439.
- Sun, D., Roth, S., and Black, M. J. (2014). “A quantitative analysis of current practices in optical flow estimation and the principles behind them,” *International Journal of Computer Vision* **106**(2), 115–137.
- Sun, D., Roth, S., Lewis, J. P., and Black, M. J. (2008). “Learning optical flow,” in *Computer Vision - ECCV 2008, 10th European Conference on Computer Vision, Marseille, France, October 12–18, 2008, Proceedings, Part III*.
- Vaudrey, T., and Klette, R. (2009). “Residual images remove illumination artifacts!,” in *DAGM Symposium on Pattern Recognition*, pp. 472–481.
- Wedel, A., Pock, T., Zach, C., Bischof, H., and Cremers, D. (2009). “An improved algorithm for TV- L^1 optical flow,” in *Statistical and Geometrical Approaches to Visual Motion Analysis*, edited by D. Cremers, B. Rosenhahn, A. L. Yuille, and F. R. Schmidt, Springer, Berlin, pp. 23–45.
- Xiang, Y., Wang, F., Wan, L., Jiao, N., and You, H. (2019). “OS-Flow: A robust algorithm for dense optical and SAR image registration,” *IEEE Transactions on Geoscience and Remote Sensing* **57**(9), 6335–6354.
- Yang, T. C., Schindall, J., Huang, C. F., and Liu, J. Y. (2012). “Clutter reduction using doppler sonar in a harbor environment,” *Journal of the Acoustical Society of America* **132**(5), 3053–3067.
- Yu, G., Yang, T. C., and Piao, S. (2017). “Estimating the delay-Doppler of target echo in a high clutter underwater environment using wideband linear chirp signals: Evaluation of performance with experimental data,” *Journal of the Acoustical Society of America* **142**(4), 2047–2057.
- Zhao, S., Han, Y., Liu, Q., and Huang, H. (2020a). “Detecting moving targets in active sonar echograph of harbor environment using high-order time lacunarity,” *Journal of the Acoustical Society of America* **147**(4), 2110–2120.
- Zhao, S., Han, Y., Wei, Z., Liu, Q., and Huang, H. (2020b). “Fast online high-order time lacunarity for characterizing active sonar echographs of harbor environment,” *The Journal of the Acoustical Society of America* **148**(5), EL401–EL407.